

RecurSeed and EdgePredictMix: Pseudo-Label Refinement Learning for Weakly Supervised Semantic Segmentation across Single- and Multi-Stage Frameworks

Sanghyun Jo¹ In-Jae Yu² Kyungsu Kim^{3*}
¹OGQ, Seoul, Korea ²Samsung Electronics, Suwon, Korea

³Department of Data Convergence and Future Medicine, Sungkyunkwan University, Seoul, Korea
 {shjo.april, iju.phd, kskim.doc}@gmail.com

Abstract

Although weakly supervised semantic segmentation using only image-level labels (WSSS-IL) is potentially useful, its low performance and implementation complexity still limit its application. The main causes are (a) non-detection and (b) false-detection phenomena: (a) The class activation maps refined from existing WSSS-IL methods still only represent partial regions for large-scale objects, and (b) for small-scale objects, over-activation causes them to deviate from the object edges. We propose *RecurSeed*, which alternately reduces non- and false detections through recursive iterations, thereby implicitly finding an optimal junction that minimizes both errors. We also propose a novel data augmentation (DA) approach called *EdgePredictMix*, which further expresses an object's edge by utilizing the probability difference information between adjacent pixels in combining the segmentation results, thereby compensating for the shortcomings when applying the existing DA methods to WSSS. We achieved new state-of-the-art performances on both the PASCAL VOC 2012 and MS COCO 2014 benchmarks (VOC val: 74.4%, COCO val: 46.4%). The code is available at https://github.com/shjo-april/RecurSeed_and_EdgePredictMix.

1. Introduction

Semantic segmentation is pivotal in computer vision image analysis. However, training these models demands pixel-wise annotations, taking about 20 seconds for image-level and 239 seconds for pixel-level annotations per image. Recent methods [23, 44] have developed weakly supervised semantic segmentation (WSSS) techniques leveraging weaker labels to lower the cost of mask labeling, like image-level class labels [1] and points [4]. Among these, we focus on WSSS using image-level class labels (WSSS-IL) as the most economical supervision.

Most WSSS-IL approaches utilize a class activation map

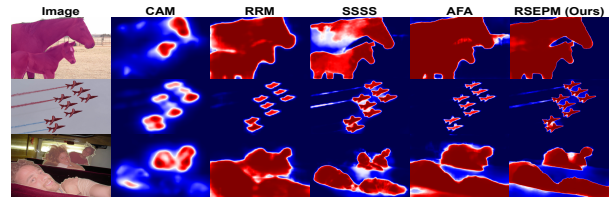


Figure 1. Comparison of localization maps produced by using conventional CAMs, existing single-stage learning frameworks, and ours, with PASCAL VOC 2012 training set. Our results show foreground and background regions more accurately than other localization maps, thanks to the recursive learning process (RS).

(CAM) [59]. However, CAM highlights the object's most discriminative regions, causing many false negatives (FNs). To mitigate CAM's limitations, recent state-of-the-art methods [7, 9, 60] adopt a multi-stage learning framework (MLF). This MLF encompasses stages tailored for specific tasks, rendering the training process intricate. Single-stage learning frameworks (SLFs) address these MLF complexities by employing a unified model. Nevertheless, current SLFs [42, 56] lag in performance compared to MLFs.

Meanwhile, post-processing modules for CAMs, such as Self-Correlation map Generation (SCG) [35] and Pixel-Adaptive Mask Refinement (PAMR) [3], leverage feature and image correlations, respectively. While SCG enhances spatial details for larger objects, it raises false positives (FPs) for medium and small objects. In contrast, PAMR effectively reduces FPs by refining the CAM's boundaries, but when used alone, it can increase FNs due to a lack of dispersion in initial CAMs. These conflicting FN and FP issues in WSSS-IL are termed FPN-WSSS-IL.

On the other hand, data augmentation (DA) is a straightforward technique that boosts data efficacy. Existing DA strategies, like ClassMix [34], enrich datasets by blending images using model-predicted masks. However, in the WSSS-IL context, implementing such mixing augmentations without refining these predicted masks escalates ambiguity stemming from the partial object boundaries present in the masks. We denote this challenge as IBDA-WSSS-IL.

*Correspondence to

Table 1. Comparison with RS and its related works to highlight our novelty: SEAM [48], RRM [56], AFA [43].

Properties	SEAM	RRM	AFA	RS (Ours)
Employ recursion principle for improving CAM	✓	✓	✓	✓
Reduce FP by using mask refinement		✓	✓	✓
Reduce FN by using the first-order correlation	✓		✓	✓
Reduce FN by using the second-order correlation				✓

To address both FPN-WSSS-IL and IBDA-WSSS-IL challenges, we introduce RecurSeed (RS) and EdgePredictMix (EPM). RS recursively refines the initial CAM by leveraging its high-order correlation (*e.g.*, SCG) along with mask refinements (*e.g.*, PAMR) during training, thereby diminishing both FP and FN in CAM, as illustrated in Fig. 1. EPM, the pioneering DA solution for IBDA-WSSS-IL, enhances uncertain pixels in mixed results by restoring edge data from the model’s predictions. Our primary contributions can be summarized as follows.

- To mitigate FPN-WSSS-IL, we *newly apply a recursion* (RS) to the integration of SCG and PAMR beyond their original post-processing roles. Unlike a simple combination for post-processing, our RS facilitates the network’s convergence towards a mask that optimally reduces both FN and FP, yielding a performance boost over 11% compared to non-recursive methods. The efficacy of RS stems from recursively transferring the knowledge of spatial information (PAMR) refined by the second-order correlation (SCG) to the network. By leveraging the high-order correlation, our RS surpasses traditional recursion methods (*i.e.*, using the first-order correlation), improving the performance by 7.4% in mIoU (see Tab. 5).
- To address IBDA-WSSS-IL, we propose a novel edge refinement (EP) optimized for mixing augmentation (EPM). To maximize the mixing effect, EPM refines predicted masks *by jointly harnessing absolute and relative per-pixel probability values*, consistently boosting the performance of various WSSS methods in Tab. 7.
- Our SLF achieves the highest performance with an mIoU of 70.6% on the VOC 2012 test set, even without utilizing advanced backbones (*e.g.*, transformers). This result demonstrates that our SLF can deliver superior performance in WSSS-IL without intricate learning configurations like MLF. When our SLF is extended straightforwardly into MLF by applying a random walk [1], our method exceeds recent MLFs [9, 53] by a 1.7% and surpasses recent methods using additional supervision, like saliency [17], on all benchmarks (see Tab. 3).

2. Related work

2.1. Weakly supervised semantic segmentation

Most studies [9, 10, 17, 18, 20, 23–26, 28, 40, 47, 49, 53, 60] have focused on improving the initial CAM quality, adopt-

Table 2. Comparison with EPM and its related DA studies to highlight our novelty: SG [37], CDA [46], ClassMix [34].

Properties	SG	CDA	ClassMix	EPM (Ours)
Use predicted mask in mix	✓	✓	✓	✓
Use mixed mask in learning			✓	✓
Consider mix in WSSS		✓		✓
Refine predicted mask using edge				✓

ing MLF that involves producing an initial CAM, generating pseudo masks, and training the segmentation model. Independent research like C^2 AM [51], ADEHE [32], and SANCE [29] aimed to rectify inaccuracies in pseudo masks. Meanwhile, W-OoD [27] and CLIMS [50] employed additional supervision, such as saliency and manually collected dataset, to address CAM’s limitations. All studies above did not consider a recursion process.

Novelty of RS. While several methods [3, 7, 43, 44, 48, 56, 58] have integrated the recursive process akin to our RecurSeed (RS), they have yet to leverage high-order correlations, causing an inadequate reduction in FN. In Tab. 1, our RS stands out in key characteristics. Specifically, approaches like SEAM [48], CPN [58], and SIPE [7] utilize first-order correlations without mask refinement, increasing FP with limited FN reductions for CAMs. Meanwhile, RRM [56] and SSSS [3] refine the typical CAM in the training loop without any feature correlation, leaving the CAM’s FN unaddressed. Employing a transformer architecture, AFA [43] developed an SLF using first-order correlation and mask refinement. Despite leveraging the inherent strengths of transformers [44], the first-order correlation leads to only a slight FN reduction in their approach. Our study also belongs to an SLF but surprisingly mitigates FP and FN *by jointly applying the high-order correlation of CAM and its subsequent refinement in the recursion principle for the first time*.

2.2. Data augmentation

CutMix [55] crops a random region of an image and pastes it on another. Saliency Grafting (SG) [37] adjusts mixed class labels based on occlusion degrees derived from the CAM’s saliency map. CDA [46] is the first DA method for improving WSSS performance. ClassMix [34] merges unlabeled images with decoder outputs by training partial pixel-wise annotations.

Novelty of EPM. Previous works have employed affine transformation [48], cropping [17], and mixing [46]. Our EdgePredictMix (EPM) is the sole method considering edge refinement to amplify the mixing effect. Specifically, our edge refinement (EP) technique enhances ambiguous pixels using edge data from uncertain regions in predicted masks. Tab. 2 compares our EPM with other DA methods regarding critical properties.

2. EdgePredictMix (Sec. 3.3)

The diagram illustrates the EdgePredictMix framework, which integrates a single-stage network with a multi-scale fusion module (SLF) and a recursive seed refinement module (RecurSeed).

Single-stage Network (Top):

- Input image I is processed by the **Encoder (Eq. 5)** and **Decoder (Eq. 8)** within **Our single-stage network**.
- The decoder produces a segmentation map \hat{M}_{dec} and a camouflage map \hat{M}_{cam} .
- \hat{M}_{dec} is compared with ground truth M_{seg} using loss $\mathcal{L}_{seg}(\hat{M}_{dec}, M_{seg})$.
- \hat{M}_{cam} is compared with ground truth M_{rs} using loss $\mathcal{L}_{rec}(\hat{M}_{cam}, M_{rs})$.
- A **1x1 Conv (Eq. 6)** is applied to \hat{M}_{cam} .
- A **GAP (Eq. 7)** is applied to \hat{M}_{dec} to produce class labels \hat{Y}_{cls} , which are compared with ground truth Y using loss $\mathcal{L}_{cls}(\hat{Y}_{cls}, Y)$.
- \hat{M}_{cam} is processed by **RecurSeed (RS) (Eq. 1)** to produce M_{rs} , which is then filtered by **CertainFilter (Eq. 9)**.

EdgePredictMix Module (Bottom):

- Two input images I_i and I_j are processed by **Our SLF** to produce $\hat{M}_{dec}^i, \hat{M}_{cam}^i$ and $\hat{M}_{dec}^j, \hat{M}_{cam}^j$.
- These are then processed by **RecurSeed (RS) (Eq. 1)** to produce **Mix RS outputs (Eq. 14)**.
- The outputs are then processed by **Edge Refinement (EP) (Eq. 10)** to produce **Mix decoder outputs (Eq. 13)**.
- The **Mix images (Eq. 12)** are processed by **Our SLF** to produce \hat{M}_{dec}^{mix} and \hat{M}_{cam}^{mix} .
- \hat{M}_{dec}^{mix} is compared with ground truth M_{seg}^{mix} using loss $\mathcal{L}_{seg}^{mix}(\hat{M}_{dec}^{mix}, M_{seg}^{mix})$.
- \hat{M}_{cam}^{mix} is compared with ground truth M_{rs}^{mix} using loss $\mathcal{L}_{rec}^{mix}(\hat{M}_{cam}^{mix}, M_{rs}^{mix})$.

Legend:

- Blue box: Our SLF (Shared parameters)
- Red arrow: Backward (Recursive Update)

The end-to-end objective function of RS+EPM

$$\mathcal{L}_{total} = \mathcal{L}_{cls} + \mathcal{L}_{seg} + \mathcal{L}_{rec} + \mathcal{L}_{seg}^{mix} + \mathcal{L}_{rec}^{mix}$$

3. Method

Our proposed method for the single-stage learning framework encompasses parallel classification and segmentation branches. We introduce two components tailored to WSSS: (i) RecurSeed (RS) and (ii) EdgePredictMix (EPM). RS iteratively updates the initial CAM, leveraging high-order and image correlations, enlarging previously undetected foregrounds. Our edge refinement (EP) removes uncertain pixels in pseudo masks using the edge details from model predictions. Subsequently, EPM merges pairs of images and EP-refined pseudo masks, facilitating sample diversity and enhancing WSSS performance. The comprehensive framework is depicted in Fig. 2.

Our application of recursive learning to baselines that utilize high-order (*e.g.*, SCG) and image correlations (*e.g.*, PAMR) adeptly mitigates FPN-WSSS-IL by imparting the semantic knowledge of refined CAMs onto the network. Without our RS, juxtaposing SCG and PAMR yields only a modest enhancement in CAM quality, as evidenced in Fig. 3(a). This approach still results in a high FN, attributed to the suboptimal initial CAMs. Our RS resolves the limitations from the direct amalgamation of SCG and PAMR by putting them firstly to the learning process, as illustrated in Fig. 3(b).

$$M_{rs}(t) = PAMR(SCG(M_{cam}(t)); \mathcal{W}), \quad (1)$$

3

tively (detailed in Appendix A), $M_{cam}(0)$ is the initial CAM, $M_{rs}(t)$ denotes its refined result through RS, and $\mathcal{W} = SCG(M_{cam}(t))$ is set as the SCG’s activation region. Thus, $M_{rs}(0)$ expressed in (1) is simply the result of sequentially applying SCG and PAMR to the CAM’s result. In particular, our contribution is that we add the recursive learning as in (4) so that CAM can reconstruct this result (RS); thanks to RS, the CAM results gradually improve as learning progressed, beyond this simple integration $M_{rs}(0)$. Intuitively, we recursively improve the result of $M_{cam}(0)$ by training the network such that the CAM updated at the next step $M_{cam}(1)$ becomes the result $M_{rs}(0)$, aiming at $M_{rs}(t) \approx M_{cam}(t+1)$ for every epoch $t \in \{0 : T\}$. As shown in Figs 3(b) and (c), our RS gradually updates the initial seed (i.e., CAMs) to remedy the shortcomings of the simple combination of SCG and PAMR in (1).

To achieve the objective of $M_{rs}(t) \approx M_{cam}(t+1)$, we minimize the reconstruction loss in (3) (i.e., in decoder domain) and (4) (i.e., in encoder domain) along with the classification loss in (2), and the total net parameter θ_t is updated at step t as follows:

$$\begin{aligned} \theta_t = \theta_{t-1} - \eta \frac{\partial}{\partial \theta} \mathbb{E}_{\mathbf{I}} [\mathcal{L}_{cls}(\hat{Y}_{cls}(\tau), \mathbf{Y}; \theta)] \Big|_{\theta=\theta_{\tau}, \tau=t-1} \\ - \eta \frac{\partial}{\partial \theta} \mathbb{E}_{\mathbf{I}} [\mathcal{L}_{seg}(\hat{M}_{dec}(\tau), M_{seg}(\tau); \theta)] \Big|_{\theta=\theta_{\tau}, \tau=t-1} \end{aligned} \quad (2)$$

$$- \eta \frac{\partial}{\partial \theta} \mathbb{E}_{\mathbf{I}} [\mathcal{L}_{rec}(\hat{M}_{cam}(\tau), M_{rs}(\tau); \theta)] \Big|_{\theta=\theta_{\tau}, \tau=t-1}, \quad (4)$$

where $\mathbf{I} = \{I^1, I^2, \dots, I^B\}$ denotes a mini-batch of size B , \mathbf{Y} denotes their truth class labels,

$$f_{enc}(t) = E_{\theta_t^{enc}}(\mathbf{I}), \quad (5)$$

$$\hat{M}_{cam}(t) = A_{\theta_t^{cls}}(f_{enc}(t)), \quad (6)$$

$$\hat{Y}_{cls}(t) = \sigma(GAP(\hat{M}_{cam}(t))), \quad (7)$$

$$\hat{M}_{dec}(t) = D_{\theta_t^{dec}}(f_{enc}(t)), \quad (8)$$

and

$$\begin{aligned} M_{seg}(t) &= CF(M_{rs}(t)) \\ &= \begin{cases} \underset{c \in \mathcal{C}}{\operatorname{argmax}}(M_{rs}^c(t)[:, i, j]) & \text{if } \max_{c \in \mathcal{C}}(M_{rs}^c(t)[:, i, j]) > \delta_{fg}, \\ 0 & \text{if } \max_{c \in \mathcal{C}}(M_{rs}^c(t)[:, i, j]) < \delta_{bg}, \\ -1 & \text{otherwise.} \end{cases} \end{aligned} \quad (9)$$

where 0 and -1 represent the background and ignored classes, respectively. As shown in Fig. 2, our network consists of an encoder $E(\cdot)$ and a decoder $D(\cdot)$ with outputs of $f_{enc}(t)$ in (5) and $\hat{M}_{dec}(t)$ in (8), respectively. The refined CAM $\hat{M}_{cam}(t)$ is then obtained as (6) by adding layer $A(\cdot)$, scaling the number of channels to the number of classes. We apply global average pooling (GAP) and sigmoid σ to estimate the class labels as $\hat{Y}_{cls}(t)$ in (7). Following the common practice, we employ the multi-label soft margin loss

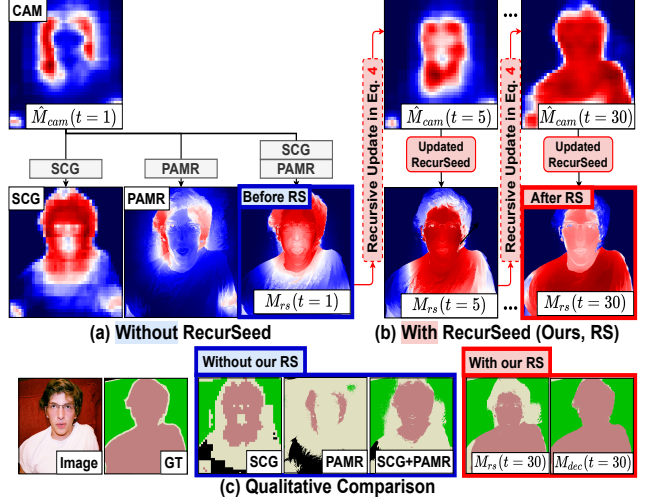


Figure 3. (a) Without our RS, the simple post-processing schemes for CAM show each output. (b) With our RS, our method iteratively improves the CAM, thereby taking advantage of both the strengths of SCG (i.e., reducing FN) and PAMR (i.e., reducing FP). (c) Quality of pseudo masks produced from CertainFilter (CF) in (9). Simple post-processing results (e.g., SCG) fail to detect integral objects precisely. By contrast, our method delineates target objects by updating the initial CAM recursively.

for the classification loss L_{cls} , the per-pixel cross-entropy loss for the segmentation loss L_{seg} , and the L1 loss for the reconstruction loss L_{rec} .

Our network narrows the gap between the decoder output $\hat{M}_{dec}(t)$ (or CAM $\hat{M}_{cam}(t)$) and RS $M_{rs}(t)$ through (3) (or (4)), leading to indirect (or direct) improvements in the CAM $\hat{M}_{cam}(t)$ in the next step as the latent feature of the decoder. For stable training, CF is applied to generate the pseudo label $M_{cl}^t = CF(M_{rs}(t))$ in (9) and to avoid the influence of uncertain labels. Through this process, CF filters certain and uncertain regions of the RS, thereby enhancing the reliability of the learning.

3.3. EdgePredictMix

We introduce EPM, a novel data augmentation method designed to address IBDA-WSSS-IL. EPM entails two primary components: mask refinement and mask synthesis. In the refinement phase, termed EP, we utilize *absolute and relative per-pixel probability values*. Specifically, we threshold the absolute class probabilities of each pixel to identify uncertain regions. Concurrently, we extract an edge from the mask by assessing the relative differences between adjacent per-pixel probability values and produce superpixels from the edge. Uncertain pixels with low absolute probabilities are then complemented by selecting the predominant class within each superpixel. For edge and superpixel extraction, we employ established algorithms, Canny [5] and Connected-component labeling (CCL) [41]. Two EP-refined masks with their associated original images are merged in the synthesis

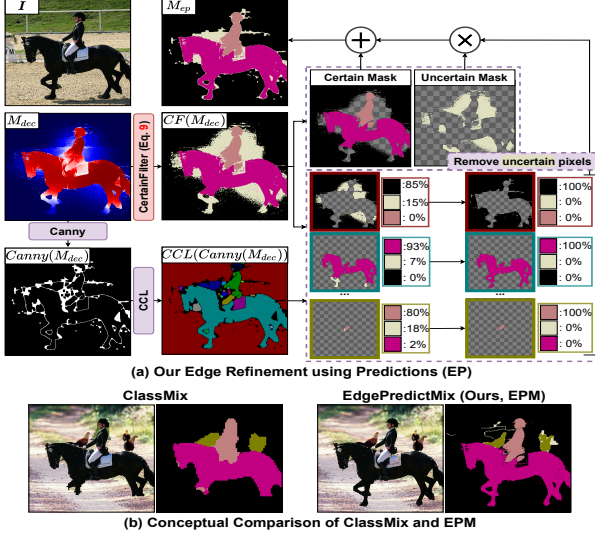


Figure 4. (a) Illustration of EP. We create a superpixel separated from the edge between class probabilities and then vote the major class within each superpixel label to remove uncertain pixels. (b) Comparison of recent mixing method (ClassMix). Our EP eliminates uncertain regions in pseudo masks by superpixel-based relabeling, significantly improving WSSS performance.

phase. The EPM process is depicted in Fig. 4 and formulated in the following steps for two arbitrary indices $i, j \in \{1 : B\}$ in a mini-batch.

The first step of EPM is to supplement the uncertain mask produced from the model by EP so that the decoder output $M_{dec}^i(t)$ in the current epoch t is converted to $M_{ep}^i(t)$ as in (10). Then, we extract the union of all EP-refined foregrounds for image I_i as \mathcal{M}_{fg}^i in (11).

$$M_{dec}^i(t) = PAMR(D_{\theta_t^{dec}}(E_{\theta_t^{enc}}(I_i)); \mathcal{W})$$

$$M_{ep}^i(t) = EP(M_{dec}^i(t)) \quad (10)$$

$$\mathcal{R}_c^i(t) = \{(k, n) \mid M_{ep}^i(t)[c, k, n] > \delta_{fg}\}$$

$$\mathcal{M}_{fg}^i = \mathbb{1}[\cup_{c \in \mathcal{C}} \mathcal{R}_c^i(t)], \quad (11)$$

where $\mathbb{1}$ denotes the element-wise indicator operator and \mathcal{W} is set as the active region of $D_{\theta_t^{dec}}(E_{\theta_t^{enc}}(I_i))$. The second step is pasting certain regions \mathcal{M}_{fg}^i of an image I_i and its corresponding EP-refined-mask set $M_{ep}^i(t)$ (or its RS seed as encoder output $M_{rs}^i(t)$) onto the image I_j and its EP-refined-mask set $M_{ep}^j(t)$ (or its RS seed $M_{rs}^j(t)$), respectively, as shown in $I_{i \rightarrow j}$ in (12) and $M_{i \rightarrow j}^{rs}(t)$ in (13) (or $M_{i \rightarrow j}^{cam}(t)$ in (14)). In other words, $I_{i \rightarrow j}$, $M_{i \rightarrow j}^{seg}(t)$, and $M_{i \rightarrow j}^{rs}(t)$ correspond to the (EP-based) synthesizing results in the original image, decoder, and encoder, respectively.

$$I_{i \rightarrow j} = I_i \odot \mathcal{M}_{fg}^i + I_j \odot (1 - \mathcal{M}_{fg}^i) \quad (12)$$

$$M_{i \rightarrow j}^{seg}(t) = M_{ep}^i(t) \odot \mathcal{M}_{fg}^i + M_{ep}^j(t) \odot (1 - \mathcal{M}_{fg}^i) \quad (13)$$

$$M_{i \rightarrow j}^{rs}(t) = M_{rs}^i(t) \odot \mathcal{M}_{fg}^i + M_{rs}^j(t) \odot (1 - \mathcal{M}_{fg}^i) \quad (14)$$

We then make the network train mixed images and labels as

follows:

$$\begin{aligned} \theta_t = & \\ \theta_{t-1} - & (*) \\ & - \eta \frac{\partial}{\partial \theta} \mathbb{E}_I [\mathcal{L}_{seg}^{mix}(\hat{M}_{dec}^{mix}(\tau), M_{seg}^{mix}(\tau); \theta)] \Big|_{\theta=\theta_{\tau}, \tau=t-1}, \\ & - \eta \frac{\partial}{\partial \theta} \mathbb{E}_I [\mathcal{L}_{rec}^{mix}(\hat{M}_{cam}^{mix}(\tau), M_{rs}^{mix}(\tau); \theta)] \Big|_{\theta=\theta_{\tau}, \tau=t-1}, \end{aligned} \quad (15)$$

$$(16)$$

where $(*)$ refers to all terms in (2), (3), and (4),

$$\mathbf{I}_{mix} = \{I_{i \rightarrow j} \mid j \sim \text{unif}(\{1 : B\}/i) \text{ for } i \in \{1 : B\}\}$$

$$M_{seg}^{mix}(t) = \{M_{i \rightarrow j}^{seg}(t) \mid I_{i \rightarrow j} \in \mathbf{I}_{mix}\} \quad (17)$$

$$\hat{M}_{dec}^{mix}(t) = D_{\theta_t^{dec}}(E_{\theta_t^{cam}}(\mathbf{I}_{mix})) \quad (18)$$

$$M_{rs}^{mix}(t) = \{M_{i \rightarrow j}^{rs}(t) \mid I_{i \rightarrow j} \in \mathbf{I}_{mix}\} \quad (19)$$

$$\hat{M}_{cam}^{mix}(t) = A_{\theta_t^{cls}}(E_{\theta_t^{cam}}(\mathbf{I}_{mix})) \quad (20)$$

Using the proposed EPM, we obtain other mini-batch \mathbf{I}_{mix} of B mixed images by selecting each sample in the mini-batch \mathbf{I} , choosing another sample randomly from the remaining samples, and mixing them. The pseudo masks and the decoder outputs for \mathbf{I}_{mix} at epoch t are given by $M_{seg}^{mix}(t)$ in (17) and $\hat{M}_{dec}^{mix}(t)$ in (18), respectively, through additional optimizations specified as follows: The first loss term in (15) (or second loss term in (16)) corresponds to the cross-entropy loss (or the reconstruction loss) that makes the decoder output $\hat{M}_{dec}^{mix}(t)$ (or the encoder output $\hat{M}_{cam}^{mix}(t)$) reproduce the mixed mask refined by EP $M_{seg}^{mix}(t)$ (or the mixed RS $M_{rs}^{mix}(t)$).

4. Experiments

4.1. Reproducibility

Details for datasets. The PASCAL VOC 2012 dataset [11] comprises 21 classes, which include a background class, and is divided into three subsets: training (1,464 images), validation (1,449 images), and test (1,456 images). Following the standard WSSS setup, e.g., [1, 48], we use an augmented training dataset with 10,582 images. The MS COCO 2014 dataset [31] consists of 81 classes with 82,783 training and 40,504 validation images. The outcomes for the PASCAL VOC 2012 validation and test sets are sourced from the official evaluation server.

Implementation details. Our single-stage learning framework (SLF) is integrated with a random walk (RW) [2] for a multi-stage learning framework. We incorporate our Certain-Filter in (9) with $\delta_{fg} = 0.55$ and $\delta_{bg} = 0.10$. Following [3], we employ ResNet-50 (R50) with DeepLabv3+ [6] for our SLF and follow a multi-scale strategy with CRF [21] during testing. We use a stochastic gradient descent optimizer with

Table 3. Performance comparison of WSSS methods in terms of mIoU (%) on PASCAL VOC 2012 and COCO 2014. * indicates the backbone of VGG-16. Sup., supervision; \mathcal{I} , image-level class labels; \mathcal{S} , the saliency supervision; \mathcal{D} , an additional dataset; \mathcal{B} , box labels; \mathcal{P} , point labels.

Method	Backbone	Sup.	VOC val	VOC test	COCO val
Single-stage learning framework using image-level supervision only					
RRM [56]	WR38	\mathcal{I}	62.6	62.9	-
SSSS [3]	WR38	\mathcal{I}	62.7	64.3	-
AFA [43]	MiT-B1	\mathcal{I}	66.0	66.3	38.9
ToCo [44]	ViT-B	\mathcal{I}	69.8	70.5	41.3
RS (Ours, single-stage)	R50	\mathcal{I}	66.5	67.9	40.0
RSEPM (Ours, single-stage)	R50	\mathcal{I}	69.5	70.6	42.2
Multi-stage learning framework using image-level supervision only					
PSA [1]	WR38	\mathcal{I}	61.7	63.7	-
IRNet [2]	R50	\mathcal{I}	63.5	64.8	-
SEAM [48]	WR38	\mathcal{I}	64.5	65.7	31.9
CONTA [57]	R101	\mathcal{I}	66.1	66.7	32.8
CDA [46]	WR38	\mathcal{I}	66.1	66.8	33.2
AdvCAM [26]	R101	\mathcal{I}	68.1	68.0	-
RIB [25]	R101	\mathcal{I}	68.3	68.6	43.8
ReCAM [8]	R101	\mathcal{I}	68.5	68.4	-
ADEHE [32]	R101	\mathcal{I}	68.6	68.9	-
AMR [39]	R101	\mathcal{I}	68.8	69.1	-
SIPE [7]	R101	\mathcal{I}	68.8	69.7	40.6
AMN [28]	R101	\mathcal{I}	69.5	69.6	44.7
MCTformer [53]	WR38	\mathcal{I}	71.9	71.6	42.0
SANCE [29]	R101	\mathcal{I}	70.9	72.2	44.7†
BECO [40]	R101	\mathcal{I}	72.1	71.8	-
ACR [23]	WR38	\mathcal{I}	71.9	71.9	45.3
OCR [9]	WR38	\mathcal{I}	72.7	72.0	42.5
RS (Ours, multi-stage)	R101	\mathcal{I}	72.8	72.8	45.8
RSEPM (Ours, multi-stage)	R101	\mathcal{I}	74.4	73.6	46.4
Multi-stage learning framework using additional supervision					
DSRG [16]	R101	$\mathcal{I}+\mathcal{S}$	61.4	63.2	26.0*
FickleNet [24]	R101	$\mathcal{I}+\mathcal{S}$	64.9	65.3	-
EDAM [49]	R101	$\mathcal{I}+\mathcal{S}$	70.9	70.6	-
CLIMS [50]	R50	$\mathcal{I}+\mathcal{D}$	69.3	68.7	-
W-OoD [27]	R101	$\mathcal{I}+\mathcal{D}$	70.7	70.1	-
L2G [17]	R101	$\mathcal{I}+\mathcal{S}$	72.1	71.7	44.2
RCA [60]	R101	$\mathcal{I}+\mathcal{S}$	72.2	72.8	36.8*
PPC [10]	R101	$\mathcal{I}+\mathcal{S}$	72.6	73.6	-
Multi-stage learning framework using different supervision					
TEL [30]	R101	\mathcal{P}	74.2	-	-
BAP [33]	R101	\mathcal{B}	79.2	-	-

a weight decay of $4e^{-5}$. The initial learning rate is set to 0.1, decreasing polynomially at 0.9. Image augmentations involve random scaling, horizontal flips, and cropping to 512×512 resolution. We conduct all experiments on a single RTX A6000 GPU using PyTorch, and our training time for PASCAL VOC 2012 concludes in under 24 hours.

4.2. Comparison with state-of-the-art approaches

Under the same supervision, our SLF method outperforms most methods, even if only RecurSeed (RS) is used, on PASCAL VOC 2012 and MS COCO 2014 datasets. The Integrating our EdgePredictMix (EPM) further elevates the performance compared to employing our RecurSeed (RS) only, proving the effectiveness of our RS and EPM.

In contrast with PASCAL VOC 2012, MS COCO 2014 is more challenging because it has four times categories and requires to detection of non-salient foreground objects. As shown in the last column of Tab. 3, even for MS COCO 2014,

Table 4. Element-wise component analysis on PASCAL VOC 2012 *train* set. With RS, SCG and SCG+PAMR denote $M_{rs}(t)$ in (1) by removing and preserving operator $PAMR(\cdot)$ throughout the training, respectively. RS indicates $t = 1$ () or 30 (✓). * denotes the decoder map result.

RS (Ours)	SCG	PAMR	mIoU	FP	FN
	✓		58.0	0.268	0.165
	✓	✓	59.3	0.225 (↓ 0.043)	0.194 (↑ 0.029)
✓	✓		65.2	0.216	0.143
✓	✓	✓	65.9	0.210 (↓ 0.006)	0.141 (↓ 0.002)
✓	✓		*67.4	*0.196	*0.141
✓	✓	✓	*70.7	*0.171 (↓ 0.025)	*0.134 (↓ 0.007)

Table 5. Effect of the second-order correlation on PASCAL VOC 2012 *train* set. All experiments are based on applying PAMR. RS indicates $t = 1$ () or 30 (✓). * denotes the decoder map result.

RS (Ours)	first-order correlation	second-order correlation	mIoU
	✓		57.6
	✓	✓	59.3 (+1.7%)
✓	✓		60.8
✓	✓	✓	65.9 (+5.1%)
✓	✓		*63.3
✓	✓	✓	*70.7 (+7.4%)

our single- and multi-stage methods achieve new state-of-the-art mIoUs of 42.2% and 46.4%, marking improvements of 0.9% and 1.1% over recent studies, respectively. Notably, on the PASCAL VOC 2012 *test* set, our single-stage method with fewer parameters (*i.e.*, R50) outperforms most multi-stage methods using the same supervision. This result underscores that the latest performance can be achieved only with a single-stage method.

4.3. Analysis

Novelty of RS. Existing SCG and PAMR studies, which use a fully trained network, were individually developed for the post-processing method on the CAM. As shown in Tab. 4, the simple integration of SCG and PAMR (*i.e.*, w. SCG and PAMR but w.o. RS) not only shows a marginal improvement but also fails to reduce FP and FN simultaneously. By contrast, our RS decreases both FP and FN by leveraging the recursive update, achieving substantial improvements (+11.4%) to the simple integration. These results indicate that RS makes both SCG and PAMR utilized as recursively together to mitigate FPN-WSSS-IL. Also, as shown in Tab. 5, we demonstrate the effect of the second-order correlation in recursion. With RS, the results from the encoder and decoder yield significant improvements (+7.4%) versus the first-order correlation. However, the second-order correlation without RS improves the first-order correlation marginally. Therefore, we verify the validity of the second-order correlation in the recursion principle, *i.e.*, the novelty of the proposed RS.

Novelty of EPM. The previous data augmentation (DA) methods rely on unsuitable seeds (*e.g.*, CAM) or ideal anno-

Table 6. Performance comparison with the proposed EPM and existing mixing methods in terms of mIoU (%) on PASCAL VOC 2012 *train* set. * denotes our implementation for a fair comparison.

Method	Backbone	mIoU
RecurSeed	R50	70.7
RecurSeed + *CutMix [55]	R50	68.5
RecurSeed + *Saliency Grafting [37]	R50	68.6
RecurSeed + *CDA [46]	R50	69.0
RecurSeed + *ClassMix [34]	R50	71.2
RecurSeed + EdgePredictMix (Ours)	R50	75.2

Table 7. Effect of our EPM with other single-stage methods on PASCAL VOC 2012 *val* set.

Method	Backbone	mIoU
RRM [56]	WR38	62.6
+ EdgePredictMix (Ours)	WR38	65.3 (+2.7%)
SSSS [3]	WR38	62.7
+ EdgePredictMix (Ours)	WR38	65.5 (+2.8%)
AEA [43]	MiT-B1	66.0
+ EdgePredictMix (Ours)	MiT-B1	68.5 (+2.5%)

tations (e.g., pixel-wise annotations). Nevertheless, we apply our RS in our EPM and other DA methods for a fair comparison. In Tab. 6, CutMix [55], Saliency Grafting [37], and CDA [46] decrease approximately 2% of mIoU. ClassMix [34] only shows a marginal improvement for the WSSS due to mixing predicted masks without mask refinement. Our EPM not only trains mixed masks (like ClassMix) but also further refines pseudo masks by leveraging the reconstituted edge from uncertain regions, thereby resulting in the highest WSSS performance (mIoU 75.2%) compared to other DA techniques (the best mIoU 71.2%).

Similar to CutMix [55], our EPM can be applied to any WSSS methods, as in Tab. 7. We use Canny [5] as it is the well-known method of edge detection. Therefore, we replace it with other methods [52]; our method shows consistent superiority regardless of edge detection methods on the PASCAL VOC 2012 *val* set. (RSEPM using Canny [5]: 69.5%, RSEPM using HED [52]: 69.4%).

Importance of the proposed components. To clarify the effect of the proposed RS and EPM, we conduct ablation studies related to loss functions and EP on our single-stage network. In Tab. 8, we report different combinations as we add or remove components. First, as shown in row 3, we observe that training both the encoder and decoder with our RS significantly improves the decoder’s performance and brings an explicit gain for the CAM as the recursively advanced features lead to better pseudo masks in the next step. In addition, RS with EP achieves 71.7% of the decoder in row 4. The result shows that EP itself achieves meaningful improvement even without mixing augmentation. Second, in rows 5 and 7, training mixed results without EP shows a certain level of improvement and outperforms ClassMix [34] as the model only trains reliable labels from CF. We present samples of qualitative segmentation results on PASCAL VOC 2012 and MS COCO 2014 sets in Appendix

Table 8. Effect of key components for the proposed RS and EPM in terms of mIoU (%) on PASCAL VOC 2012 *train* set.

	L_{cls}	L_{seg}	L_{rec}	L_{seg}^{mix}	L_{rec}^{mix}	EP	CAM	Decoder
	RecurSeed			EdgePredictMix				
1	✓						46.9	17.4
2	✓	✓					51.6	65.8
3	✓	✓	✓				57.9	70.7
4	✓	✓	✓			✓	59.0	71.7
5	✓	✓	✓	✓			61.0	73.5
6	✓	✓	✓	✓		✓	60.8	74.5
7	✓	✓	✓	✓	✓		61.9	73.6
8	✓	✓	✓	✓	✓	✓	63.4	75.2

Table 9. mIoUs (%) of single-stage results produced from a trained network (Seed) and pseudo masks generated by RW [2] on PASCAL VOC 2012 *train* set.

Method	Backbone	Seed	Seed + RW
SEAM [48]	WR38	55.4	63.6
IRNet [2]	R50	48.8	66.3
CDA [46]	R50	50.8	67.7
CPN [58]	WR38	57.4	67.8
CONTA [57]	R50	48.8	67.9
AdvCAM [26]	R50	55.6	69.9
PPC [10]	WR38	61.5	70.1
RIB [25]	R50	56.5	70.6
RS (Ours)	R50	70.7	74.8
RSEPM (Ours)	R50	75.2	76.7

C.2. In the last row, we achieve the best performance when applying essential components together with EP by exploiting absolute and relative per-pixel probability information. Therefore, we demonstrate the novelty and validity of the proposed components (*i.e.*, RS and EPM).

Additional comparison with existing MLFs using RW.

In Tab. 9, we compare the performance of the proposed SLF with existing MLFs [2, 25, 48] by extending it to MLF with the same configuration of RW. Surprisingly, in all cases before or after the application of RW, our method outperforms the related works by achieving mIoUs of 75.2% and 76.7% without and with RW, respectively, exhibiting the performance improvement of at least 15% and 6% compared to the prior arts (CPN 57.4% and RIB 70.6% respectively). This also proves the superiority of the proposed RS and EPM.

Hyperparameter analysis. To validate the effects of the proposed RS and EPM, we evaluate our single-stage results for each epoch, as shown in Fig. 5(a). Initially, the mIoU increases steeply through the RS between the 5th and 10th epochs. However, the mIoU then saturates between the 10th and 15th epochs. To address this saturation, we apply EPM after the 15th epoch. Here, δ_{fg} and δ_{bg} in (9) control the foreground and background regions. Although we observe a sufficiently high mIoU above a certain level irrespective of changes of δ_{fg} and δ_{bg} in Figs 5(b)-(c), the best performance can be found through their adjustment, proving the validity of two thresholds.

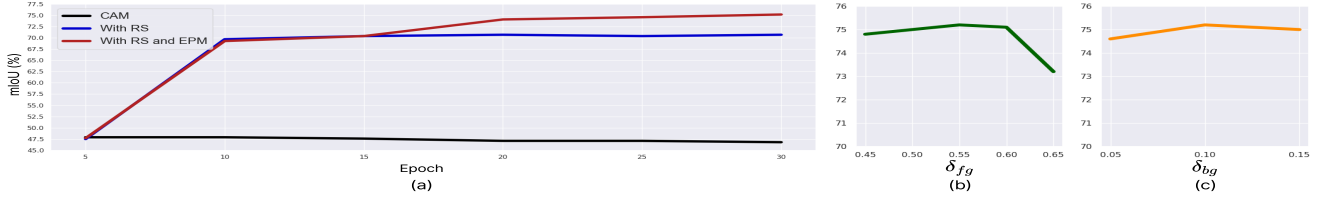


Figure 5. (a) Effects of RS and EPM per epoch. (b) Effect of foreground threshold δ_{fg} . (c) Effect of background threshold δ_{bg} .

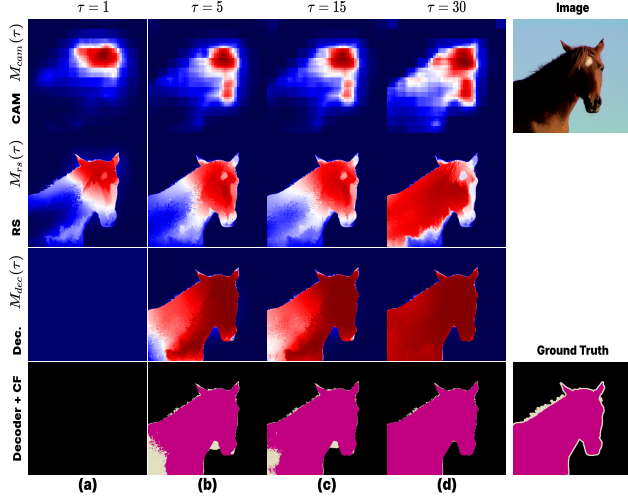


Figure 6. Visualization of attention maps and pseudo masks with recursive improvements.

Qualitative improvements. Fig. 6 illustrates the results produced by our single-stage method (including CAM, RS, and Decoder). We then generate pseudo masks from the decoder output by using CF. For the initial training step shown in Fig. 6(a), CAM and SCG cover the most discriminative part of an object. In addition, the decoder output from the segmentation branch fails to detect all of the foregrounds owing to insufficient training steps. After we apply RS to train the segmentation branch (Figs 6(b)-(c)), the predicted masks are better than those at the initial step ($t = 1$). As the learning steps progress through EPM (Fig. 6(d)), the CAM and SCG represent more integral regions of an object, and the segmentation branch produces an accurate seed. Specifically, we secure the data diversity and increase the mIoU by more than 5%. The qualities of pseudo masks (Decoder+CF) are improved progressively in Figs 6(a)-(d), and the final mask in Fig. 6(d) is then close to the ground truth.

Qualitative results. We present some examples of qualitative segmentation results produced by our method on both the PASCAL VOC 2012 and MS COCO 2014 *val* sets in Fig. 7, respectively. These results show that our method not only performs well for different complex scenes, small objects, or multiple instances but also can achieve a satisfactory segmentation performance for various challenging scenes.

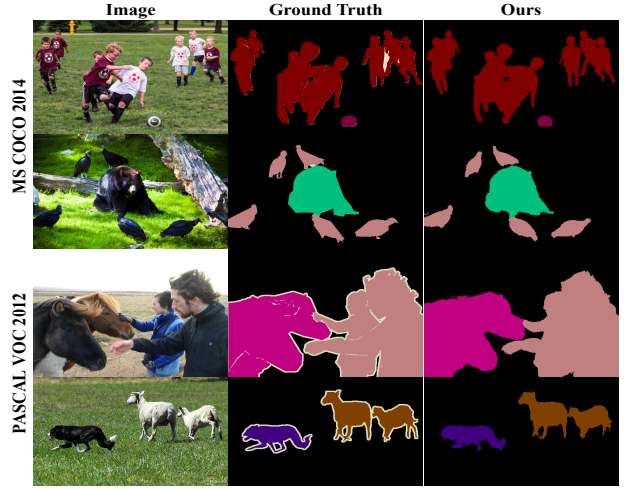


Figure 7. Qualitative results on the VOC and COCO *val* sets.

Table 10. Comparison with ours and other single-stage methods on PASCAL VOC 2012 *test* set.

Method	Backbone	Params (M)	MACs (G)	mIoU
RRM [56]	WR38	124	3990	62.9
SSSS [3]	WR38	137	678	64.3
AFA [43]	MiT-B1	14	52	66.3
ToCo [44]	ViT-B	106	250	70.5
RSEPM (Ours)	R50	40	32	70.6

Complexity. Tab. 10 shows our efficiency. Ours outperforms previous studies while using fewer parameters. The proposed RS and EPM are only used for training, so our method does not require extra complexity at inference time.

5. Conclusion

In this study, we proposed RecurSeed (RS) and EdgePredict-Mix (EPM) to improve the WSSS-IL performance, achieving new state-of-the-art performances on the PASCAL VOC 2012 and MS COCO 2014 benchmarks. Furthermore, because RS and EPM are learning methods generally applicable to SLFs consisting of an arbitrary encoder and decoder, one can upgrade this backbone to achieve a higher SLF performance. We also expect higher MLF performance can be derived by performing multi-stage extension from the proposed SLF to the latest techniques other than a random walk (RW) or applying our RS and EPM to the individual learning of any recent MLF. From this perspective, we expect that our single- and multi-stage methods have high utility and scalability in weakly or semi-supervised tasks.

A. Background

A.1. SCG

The self-correlation map generating module (SCG) [35] exploits the second-order self-correlation (SC) of the feature maps to extract their inherent structural information. SCG uses the first- and second-order SCs $SC_l^1, SC_l^2 \in \mathbb{R}^{hw \times hw}$ for a given feature map $f^l \in \mathbb{R}^{hw \times u}$ of the l -th layer of the network.

$$SC_l^1[i, j, :, :] = \text{ReLU}\left(\frac{f_i^l \top f_j^l}{\|f_i^l\| \|f_j^l\|}\right),$$

$$SC_l^2[i, :, :, :] = \text{mnm}x_j\left(\text{avg}_k\left[\frac{f_i^l \top f_k^l}{\|f_i^l\| \|f_k^l\|} \odot \frac{f_k^l \top f_j^l}{\|f_k^l\| \|f_j^l\|}\right]\right),$$

where $\text{mnm}x_j$ denotes the min-max normalization operator along the j -th axis, avg_k denotes the function taking the mean along the k -th axis, and \odot denotes the element-wise product. Then, SCG combines the first- and second-order SCs for L different layers into the following SC, called HSC :

$$HSC = \frac{1}{L} \sum_{l=1}^L \max(SC_l^1, SC_l^2),$$

and applies HSC to obtain the refined CAM as $M_{scg} = SCG(M_{cam})$. In addition, the proposed RS includes the SCG in the training loop to maximize the effectiveness of the SCG. However, the SCG is designed to reduce the FNs of the CAM only at the inference time. We additionally reported the effects of the high-order feature correlation for SCG in Appendix.

$$M_{scg} = SCG(M_{cam})$$

$$= \text{ReLU}(K_{scg}(\{M_{cam}\}_{>\delta_h}) - K_{scg}(\{M_{cam}\}_{<\delta_l})),$$

where $\{M_{cam}\}_{>\delta_h}$ denotes the set of (i, j) indices satisfying $M_{cam}[i, j] > \delta_h$ and $K_{scg}(\{M_{cam}\}_{>\delta_h})$ denotes the average activation maps generated from each pixel in $\{M_{cam}\}_{>\delta_h}$ based on the HSC ,

$$K_{scg}(\{M\}_{\leq \delta}) = \frac{1}{|\{M\}_{\leq \delta}|} \sum_{(i,j) \in \{M\}_{\leq \delta}} HSC[i, j, :, :].$$

A.2. PAMR

Pixel-adaptive mask refinement (PAMR) proposed by [3] iteratively refines the CAM M_{cam} as $M_{pamr} = G_T(M_{cam})$ by exploiting the image pixel-level affinity matrix $(\alpha_{i,j,k,n})_{(k,n) \in \mathcal{N}(i,j)}$ for $(i, j) \in \mathcal{W} = \{1 : h, 1 : w\}$ of all pixels:

$$M_{pamr} = \text{PAMR}(M_{cam}; \mathcal{W}) = G_T(M_{cam}), \quad (21)$$

where $G_0(M_{cam}) = M_{cam}$, $G_t(M_{cam})[i, j] = \sum_{(k,n) \in \mathcal{N}(i,j)} \alpha_{i,j,k,n} M_{cam}(k, n)$, $\alpha_{i,j,k,n} = \exp[\bar{k}(i, j, k, n)] / \sum_{(q,r) \in \mathcal{N}(i,j)} \exp[\bar{k}(i, j, q, r)]$. Here,

Table 11. mIoUs (%) of CAM, SCG, and the prediction from the segmentation branch (Decoder) on PASCAL VOC 2012 and MS COCO 2014 *train* images. RS, RecurSeed; EPM, EdgePredictMix.

Dataset	RS	EPM	CAM	SCG	Decoder
VOC	✓		47.4	58.0	17.4
	✓	✓	57.9	65.9	70.7
			63.4	69.0	75.2
COCO	✓		32.1	37.8	10.6
	✓	✓	40.0	41.5	47.2
			42.3	43.2	50.3

$\bar{k}(\cdot)$ is the average affinity value $k(\cdot)$ across the RGB channels, $k(i, j, k, n) = -|I_{i,j} - I_{k,n}| / \sigma_{i,j}^2$ denotes the normalized distance between the i, j -th and k, n -th pixel values, $I_{i,j}$ denotes the i, j -th pixel value of the original image I , and $\sigma_{i,j}$ denotes the standard deviation of the image intensity computed locally for the affinity kernel. In addition, $G_T(M_{cam})[i, j]$ for $(i, j) \notin \mathcal{W}$ is set to zero.

Compared with existing methods (e.g., CRF [21]), PAMR effectively reduces the computational complexity by narrowing the affinity kernel computation $\alpha_{i,j,k,n}$ to regions of contiguous pixels $(k, n) \in \mathcal{N}(\cdot, \cdot)$ rather than all pixels $\{1 : h, 1 : w\}$.

B. Additional analysis

B.1. Effect of joint consideration for RecurSeed and EdgePredictMix

To show the effects of RecurSeed (RS) and EdgePredictMix (EPM), we conduct ablation studies with and without RS and EPM individually on our single-stage network. Without RS and EPM, training is conducted only by minimizing the classification loss L_{cls} . Tab. 11 compares the network's CAM, SCG, and decoder results for up to 30 epochs. For the PASCAL VOC 2012 and MS COCO 2014 datasets, we observe an additional improvement in the mIoU of CAM and SCG results by approximately 3%–5% with each sequential application of RS and EPM, thereby demonstrating the individual necessity and effectiveness of RS and EPM. In addition, we verify the validity of the proposed decoder by showing that its results were consistently better than those of CAM and SCG by more than approximately 5%.

B.2. Effect of high-order feature correlation in RecurSeed

In Tab. 12, we show the SCG results obtained by varying the layer combination in the HSC . For each combination, we display the mIoU of both cases, i.e., the first case in which the SCG result is generated from the raw CAM (i.e., $t = 1$) and the second case in which the SCG result is updated by the proposed RS (i.e., $t = 30$). In both cases, we observe that combining more layers in HSC sequentially improves the mIoU (i.e., from 49.7% to 58.0% for $t = 1$, and 67.5% to 69.0% for $t = 30$). From this observation, we use all layers

Table 12. Ablation study for each combination of the SCG. Our method boosts the overall performance of SCG applied in various layers. ✓ indicates that SCG is applied. L5, L4, L3, L2, and L1 means layer5, layer4, layer3, layer2, and layer1, respectively.

L5	L4	L3	L2	L1	$\tau=1$ (w.o. RS and EPM)	$\tau=30$ (w. RS and EPM)
✓					49.7	67.5
✓	✓				57.0	68.4
✓	✓	✓			57.7	68.8
✓	✓	✓	✓		57.9	69.0
✓	✓	✓	✓	✓	58.0	69.0

Table 13. Extended results of Tab. 12 with mIoU, FP, and FN: w/o RS ($t = 1$), w/ RS ($t = 30$), L5 (layer5), and L4-L1 (layers 4+3+2+1).

RS	EPM	Low L5	High L4-L1	mIoU	FP	FN
		✓		49.7	0.358	0.159
		✓	✓	58.0	0.268 (\downarrow 0.090)	0.165 (\uparrow 0.006)
✓		✓		61.9	0.232	0.161
✓		✓	✓	65.9	0.210 (\downarrow 0.022)	0.141 (\downarrow 0.020)
✓	✓	✓		67.5	0.188	0.148
✓	✓	✓	✓	69.0	0.187 (\downarrow 0.001)	0.133 (\downarrow 0.015)

from layer1 to layer5 for training the RS. In particular, the proposed RS and EPM consistently improve the performance under all combinations of layers (*e.g.*, the performance improves by 11%, from 58.0% to 69.0%, when combining all layers), validating the usefulness of our method.

In Tab. 13, we add both FN and FP results into Tab. 12. Note that the closer the network layer is to the input, the more discriminative feature maps are extracted. Therefore, using high-order features (*i.e.*, adding low layer maps L4-L1) reduces FP as it focuses on the target’s discriminative area; however, it has the side effect of increasing FN in general. If RS is not used, this trend appears as shown in Tab. 12, but if RS is used, FP decreased (0.232 \rightarrow 0.210) without increasing FN (0.161 \rightarrow 0.141). As RS repeatedly gives diverse discriminative information to the network, the network can ideally accumulate all this information, thus compensating for the weakness of increasing FN. As such, RS does not increase FN but does not play a key role in reducing FN. However, it can be observed in Tab. 13 that FN is also significantly reduced (0.148 \rightarrow 0.133) when EPM is added to RS. The reason is that EPM can effectively reduce FN by letting the network better recognize a detailed region of each object. As a result, both FN and FP achieve the lowest values of 0.133 and 0.187, respectively, when RS and EPM are considered together.

B.3. Hyperparameters for Canny.

To identify non-relevant and strong edges, we set low (10) and high (100) thresholds for Canny and 4-connectivity for Connected-component labeling (CCL) [41]. We conduct Canny’s parametric ablation study, as in Fig. 8, which shows our method is not sensitive to changing Canny’s thresholds.

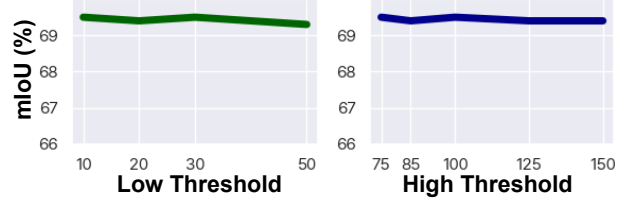


Figure 8. Sensitivity of low and high thresholds in Canny [Canny, 1986] on PASCAL VOC 2012 *val* set.

C. Additional results

C.1. Quantitative results.

We show the per-class segmentation results from the both PASCAL VOC 2012 and MS COCO 2014 datasets in Tabs. 14, 15, and 16. These quantitative results indicate that our method outperforms existing state-of-the-art methods in most class categories.

C.2. Qualitative results.

We present additional examples of qualitative segmentation results produced by our method on both the PASCAL VOC 2012 and MS COCO 2014 *val* sets in Figs. 9 and 10, respectively. These results show that our method not only performs well for different complex scenes, small objects, or multiple instances but also can achieve a satisfactory segmentation performance for various challenging scenes. We also visualize more examples of attention maps for each step ($t = 1, 5, 15, 30$) on the PASCAL VOC 2012 and MS COCO 2014 *train* sets, as shown in Figs. 11 and 12, respectively. The raw CAMs without RecurSeed (RS) (*i.e.*, $t = 1$) only focus on the local discriminative parts for large-scale objects, such as the head and hands of people or wheels of the vehicles. However, when applying the proposed RS (*i.e.*, $t = 5, 15$), our single-stage results cover more object regions, including those less discriminative regions for large-scale objects, and also capture the exact boundaries of small-scale objects (*i.e.*, decreasing the FP). Furthermore, with more training steps, including the proposed EdgePredictMix (EPM) (*i.e.*, $t = 30$), our final results produce more accurate boundaries. This demonstrates the sequential improvements through the proposed RS and EPM.

Table 14. Per-class performance comparisons with WSSS methods in terms of IoUs (%) on the PASCAL VOC 2012 *val* set.

Method	bkg	aero	bike	bird	boat	bottle	bus	car	cat	chair	cow	table	dog	horse	mbk	person	plant	sheep	sofa	train	tv	mIoU
EM-Adapt [36]	67.2	29.2	17.6	28.6	22.2	29.6	47.0	44.0	44.2	14.6	35.1	24.9	41.0	34.8	41.6	32.1	24.8	37.4	24.0	38.1	31.6	33.8
MIL-LSE [38]	79.6	50.2	21.6	40.9	34.9	40.5	45.9	51.5	60.6	12.6	51.2	11.6	56.8	52.9	44.8	42.7	31.2	55.4	21.5	38.8	36.9	42.0
SEC [20]	82.4	62.9	26.4	61.6	27.6	38.1	66.6	62.7	75.2	22.1	53.5	28.3	65.8	57.8	62.3	52.5	32.5	62.6	32.1	45.4	45.3	50.7
TransferNet [14]	85.3	68.5	26.4	69.8	36.7	49.1	68.4	55.8	77.3	6.2	75.2	14.3	69.8	71.5	61.1	31.9	25.5	74.6	33.8	49.6	43.7	52.1
CRF-RNN [42]	85.8	65.2	29.4	63.8	31.2	37.2	69.6	64.3	76.2	21.4	56.3	29.8	68.2	60.6	66.2	55.8	30.8	66.1	34.9	48.8	47.1	52.8
WebCrawl [15]	87.0	69.3	32.2	70.2	31.2	58.4	73.6	68.5	76.5	26.8	63.8	29.1	73.5	69.5	66.5	70.4	46.8	72.1	27.3	57.4	50.2	58.1
DSRG [16]	-	-	-	-	-	-	-	-	-	-	-	-	-	-	-	-	-	-	-	-	-	61.4
PSA [1]	87.6	76.7	33.9	74.5	58.5	61.7	75.9	72.9	78.6	18.8	70.8	14.1	68.7	69.6	69.5	71.3	41.5	66.5	16.4	70.2	48.7	59.4
FickleNet [24]	89.5	76.6	32.6	74.6	51.5	71.1	83.4	74.4	83.6	24.1	73.4	47.4	78.2	74.0	68.8	73.2	47.8	79.9	37.0	57.3	64.6	64.9
SSDD [45]	89.0	62.5	28.9	83.7	52.9	59.5	77.6	73.7	87.0	34.0	83.7	47.6	84.1	77.0	73.9	69.6	29.8	84.0	43.2	68.0	53.4	64.9
MCIS [47]	-	-	-	-	-	-	-	-	-	-	-	-	-	-	-	-	-	-	-	-	-	66.2
RRM [56]	87.9	75.9	31.7	78.3	54.6	62.2	80.5	73.7	71.2	30.5	67.4	40.9	71.8	66.2	70.3	72.6	49.0	70.7	38.4	62.7	58.4	62.6
SSSS [3]	88.7	70.4	35.1	75.7	51.9	65.8	71.9	64.2	81.1	30.8	73.3	28.1	81.6	69.1	62.6	74.8	48.6	71.0	40.1	68.5	64.3	62.7
CONTA [57]	-	-	-	-	-	-	-	-	-	-	-	-	-	-	-	-	-	-	-	-	-	66.1
SEAM [48]	88.8	68.5	33.3	85.7	40.4	67.3	78.9	76.3	81.9	29.1	75.5	48.1	79.9	73.8	71.4	75.2	48.9	79.8	40.9	58.2	53.0	64.5
CIAN [12]	88.2	79.5	32.6	75.7	56.8	72.1	85.3	72.9	81.7	27.6	73.3	39.8	76.4	77.0	74.9	66.8	46.6	81.0	29.1	60.4	53.3	64.3
NSRM [54]	-	-	-	-	-	-	-	-	-	-	-	-	-	-	-	-	-	-	-	-	-	68.3
EDAM [49]	-	-	-	-	-	-	-	-	-	-	-	-	-	-	-	-	-	-	-	-	-	70.9
AdvCAM [26]	90.0	79.8	34.1	82.6	63.3	70.5	89.4	76.0	87.3	31.4	81.3	33.1	82.5	80.8	74.0	72.9	50.3	82.3	42.2	74.1	52.9	68.1
CSE [22]	-	-	-	-	-	-	-	-	-	-	-	-	-	-	-	-	-	-	-	-	-	68.4
DRS [19]	-	-	-	-	-	-	-	-	-	-	-	-	-	-	-	-	-	-	-	-	-	70.4
CPN [58]	89.9	75.0	32.9	87.8	60.9	69.4	87.7	79.4	88.9	28.0	80.9	34.8	83.4	79.6	74.6	66.9	56.4	82.6	44.9	73.1	45.7	67.8
RIB [25]	90.3	76.2	33.7	82.5	64.9	73.1	88.4	78.6	88.7	32.3	80.1	37.5	83.6	79.7	75.8	71.8	47.5	84.3	44.6	65.9	54.9	68.3
Ours (single-stage, RS)	89.7	80.0	36.1	87.7	40.1	65.2	82.6	75.3	88.6	30.1	74.4	48.9	82.9	79.0	75.0	80.9	46.0	75.7	47.1	52.1	58.3	66.5
Ours (single-stage, RSEPM)	91.3	85.7	40.0	88.1	52.7	67.3	85.9	80.1	89.2	32.4	78.5	48.7	83.9	81.2	77.3	84.7	52.2	83.3	46.7	51.2	59.4	69.5
Ours (multi-stage, RS)	91.7	85.0	32.5	87.5	48.3	79.4	91.7	83.0	92.5	38.2	88.2	60.8	89.7	86.2	79.9	83.3	56.0	85.3	57.2	55.5	56.3	72.8
Ours (multi-stage, RSEPM)	92.2	88.4	35.4	87.9	63.8	79.5	93.0	84.5	92.7	39.0	90.5	54.5	90.6	87.5	83.0	84.0	61.1	85.6	52.1	56.2	60.2	74.4

Table 15. Per-class performance comparisons with WSSS methods in terms of IoUs (%) on the PASCAL VOC 2012 *test* set.

Method	bkg	aero	bike	bird	boat	bottle	bus	car	cat	chair	cow	table	dog	horse	mbk	person	plant	sheep	sofa	train	tv	mIoU
EM-Adapt [36]	76.3	37.1	21.9	41.6	26.1	38.5	50.8	44.9	48.9	16.7	40.8	29.4	47.1	45.8	54.8	28.2	30.0	44.0	29.2	34.3	46.0	39.6
MIL-LSE [38]	78.7	48.0	21.2	31.1	28.4	35.1	51.4	55.5	52.8	7.8	56.2	19.9	53.8	50.3	40.0	38.6	27.8	51.8	24.7	33.3	46.3	40.6
SEC [20]	83.5	56.4	28.5	64.1	23.6	46.5	70.6	58.5	71.3	23.2	54.0	28.0	68.1	62.1	70.0	55.0	38.4	58.0	39.9	38.4	48.3	51.7
TransferNet [14]	85.7	70.1	27.8	73.7	37.3	44.8	71.4	53.8	73.0	6.7	62.9	12.4	68.4	73.7	65.9	27.9	23.5	72.3	38.9	45.9	39.2	51.2
CRF-RNN [42]	85.7	58.8	30.5	67.6	24.7	44.7	74.8	61.8	73.7	22.9	57.4	27.5	71.3	64.8	72.4	57.3	37.3	60.4	42.8	42.2	50.6	53.7
WebCrawl [15]	87.2	63.9	32.8	72.4	26.7	64.0	72.1	70.5	77.8	23.9	63.6	32.1	77.2	75.3	76.2	71.5	45.0	68.8	35.5	46.2	49.3	58.7
DSRG [16]	-	-	-	-	-	-	-	-	-	-	-	-	-	-	-	-	-	-	-	-	-	63.2
PSA [1]	89.1	70.6	31.6	77.2	42.2	68.9	79.1	66.5	74.9	29.6	68.7	56.1	82.1	64.8	78.6	73.5	50.8	70.7	47.7	63.9	51.1	63.7
FickleNet [24]	90.3	77.0	35.2	76.0	54.2	64.3	76.6	76.1	80.2	25.7	68.6	50.2	74.6	71.8	78.3	69.5	53.8	76.5	41.8	70.0	54.2	65.0
SSDD [45]	89.5	71.8	31.4	79.3	47.3	64.2	79.9	74.6	84.9	30.8	73.5	58.2	82.7	73.4	76.4	69.9	37.4	80.5	54.5	65.7	50.3	65.5
MCIS [47]	-	-	-	-	-	-	-	-	-	-	-	-	-	-	-	-	-	-	-	-	-	66.9
RRM [56]	87.8	77.5	30.8	71.7	36.0	64.2	75.3	70.4	81.7	29.3	70.4	52.0	78.6	73.8	74.4	72.1	54.2	75.2	50.6	42.0	52.5	62.9
SSSS [3]	88.7	70.4	35.1	75.7	51.9	65.8	71.9	64.2	81.1	30.8	73.3	28.1	81.6	69.1	62.6	74.8	48.6	71.0	40.1	68.5	64.3	62.7
CONTA [57]	-	-	-	-	-	-	-	-	-	-	-	-	-	-	-	-	-	-	-	-	-	66.7
SEAM [48]	88.8	68.5	33.3	85.7	40.4	67.3	78.9	76.3	81.9	29.1	75.5	48.1	79.9	73.8	71.4	75.2	48.9	79.8	40.9	58.2	53.0	64.5
NSRM [54]	-	-	-	-	-	-	-	-	-	-	-	-	-	-	-	-	-	-	-	-	-	68.5
EDAM [49]	-	-	-	-	-	-	-	-	-	-	-	-	-	-	-	-	-	-	-	-	-	70.6
AdvCAM [26]	90.1	81.2	33.6	80.4	52.4	66.6	87.1	80.5	87.2	28.9	80.1	38.5	84.0	83.0	79.5	71.9	47.5	80.8	59.1	65.4	49.7	68.0
CSE [22]	-	-	-	-	-	-	-	-	-	-	-	-	-	-	-	-	-	-	-	-	-	68.2
DRS [19]	-	-	-	-	-	-	-	-	-	-	-	-	-	-	-	-	-	-	-	-	-	70.7
CPN [58]	90.4	79.8	32.9	85.7	52.8	66.3	87.2	81.3	87.6	28.2	79.7	50.1	82.9	80.4	78.8	70.6	51.1	83.4	55.4	68.5	44.6	68.5
RIB [25]	90.4	80.5	32.8	84.9	59.4	69.3	87.2	83.5	88.3	31.1	80.4	44.0	84.4	82.3	80.9	70.7	43.5	84.9	55.9	59.0	47.3	68.6
Ours (single-stage, RS)	89.8	83.8	33.4	87.5	39.8	67.1	85.2	78.5	91.2	29.3	77.9	54.1	84.3	81.7	78.5	78.9	53.4	78.4	53.9	42.2	56.9	67.9
Ours (single-stage, RSEPM)	91.2	86.8	37.3	80.6	52.1	71.3	87.8	81.3	90.9	32.2	80.4	54.5	86.4	88.6	83.6	80.8	59.0	82.8	54.2	42.6	59.1	70.6
Ours (multi-stage, RS)	91.4	89.5	36.2	88.7	46.2	69.1	93.1	85.7	91.8	34.0	86.7	66.3	89.0	88.8	82.9	81.3	57.3	89.0	57.5	46.9	57.9	72.8
Ours (multi-stage, RSEPM)	91.9	89.7	37.3	88.0	62.5	72.1	93.5	85.6	90.2	36.3	88.3	62.5	86.3	89.1	82.9	81.2	59.7	89.2	56.2	44.5	59.4	73.6

Table 16. Per-class performance comparisons with WSSS methods in terms of IoUs (%) on the MS COCO 2014 *val* set.

Class	SEC	DSRG	Ours (RS)	Ours (RSEPM)	Class	SEC	DSRG	Ours (RS)	Ours (RSEPM)
background	74.3	80.6	82.6	83.6	wine glass	22.3	24.0	37.5	39.8
person	43.6	-	74.8	74.9	cup	17.9	20.4	39.1	38.9
bicycle	24.2	30.4	53.1	55.0	fork	1.8	0.0	19.9	4.9
car	15.9	22.1	48.6	50.1	knife	1.4	5.0	19.9	9.0
motorcycle	52.1	54.2	72.4	72.9	spoon	0.6	0.5	5.5	1.1
airplane	36.6	45.2	73.4	76.5	bowl	12.5	18.8	26.8	11.3
bus	37.7	38.7	71.2	72.5	banana	43.6	46.4	66.4	67.0
train	30.1	33.2	44.8	47.4	apple	23.6	24.3	43.0	49.2
truck	24.1	25.9	46.5	46.5	sandwich	22.8	24.5	39.7	33.7
boat	17.3	20.6	32.1	44.1	orange	44.3	41.2	59.8	62.3
traffic light	16.7	16.1	23.6	60.8	broccoli	36.8	35.7	46.5	50.4
fire hydrant	55.9	60.4	79.0	80.3	carrot	6.7	15.3	35.1	35.0
stop sign	48.4	51.0	79.0	84.1	hot dog	31.2	24.9	49.0	48.3
parking meter	25.2	26.3	72.2	77.8	pizza	50.9	56.2	69.9	68.6
bench	16.4	22.3	40.3	41.2	donut	32.8	34.2	62.6	62.3
bird	34.7	41.5	65.2	62.6	cake	12.0	6.9	50.7	48.3
cat	57.2	62.2	79.2	79.2	chair	7.8	9.7	26.9	28.9
dog	45.2	55.6	73.4	73.3	couch	5.6	17.7	47.0	44.9
horse	34.4	42.3	74.4	76.1	potted plant	6.2	14.3	20.3	16.9
sheep	40.3	47.1	76.4	80.0	bed	23.4	32.4	54.8	53.6
cow	41.4	49.3	78.4	79.3	dining table	0.0	3.8	31.4	24.6
elephant	62.9	67.1	84.7	85.6	toilet	38.5	43.6	71.1	71.1
bear	59.1	62.6	84.9	82.9	tv	19.2	25.3	49.5	49.9
zebra	59.8	63.2	85.2	87.0	laptop	20.1	21.1	57.0	56.6
giraffe	48.8	54.3	79.8	82.2	mouse	3.5	0.9	7.9	17.4
backpack	0.3	0.2	21.6	9.4	remote	17.5	20.6	50.3	54.8
umbrella	26.0	35.3	71.1	73.4	keyboard	12.5	12.3	51.1	48.8
handbag	0.5	0.7	9.3	4.6	cell phone	32.1	33.0	61.2	60.8
tie	6.5	7.0	18.0	17.2	microwave	8.2	11.2	47.7	43.6
suitcase	16.7	23.4	54.6	53.9	oven	13.7	12.4	42.2	38.0
frisbee	12.3	13.0	55.1	57.7	toaster	0.0	0.0	0.2	0.0
skis	1.6	1.5	9.0	8.2	sink	10.8	17.8	38.8	36.9
snowboard	5.3	16.3	28.6	24.7	refrigerator	4.0	15.5	59.4	51.8
sports ball	7.9	9.8	24.5	41.6	book	0.4	12.3	28.6	27.3
kite	9.1	17.4	31.2	62.6	clock	17.8	20.7	27.8	23.3
baseball bat	1.0	4.8	1.4	1.5	vase	18.4	23.9	27.1	26.0
baseball glove	0.6	1.2	1.1	0.4	scissors	16.5	17.3	46.6	47.1
skateboard	7.1	14.4	30.4	34.8	teddy bear	47.0	46.3	69.2	68.8
surfboard	7.7	13.5	11.1	17.0	hair drier	0.0	0.0	0.0	0.0
tennis racket	9.1	6.8	14.8	9.0	toothbrush	2.8	2.0	23.3	19.7
bottle	13.2	22.3	41.3	38.1	mIoU	22.4	26.0	45.8	46.4

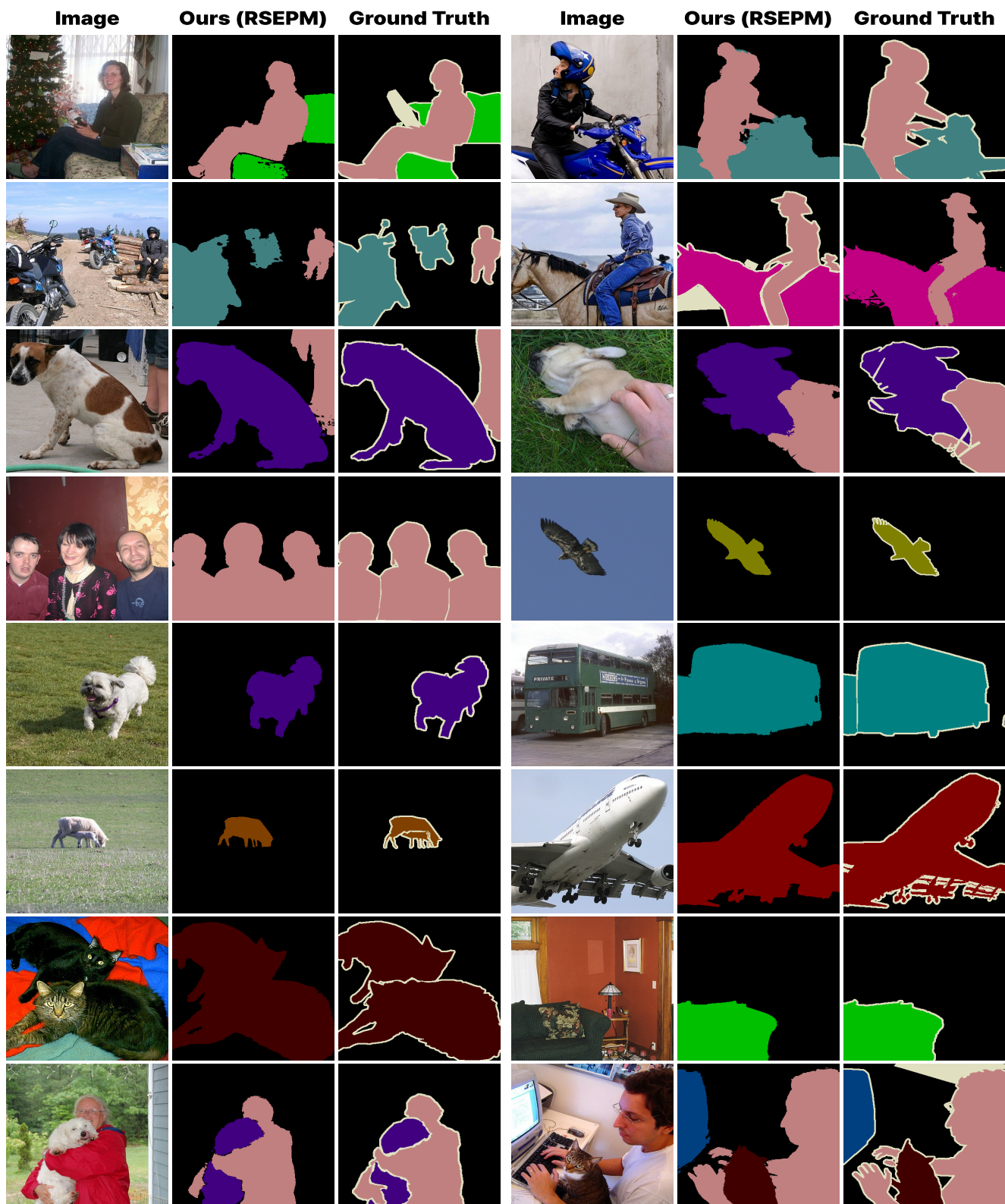


Figure 9. Qualitative segmentation results of PASCAL VOC 2012 *val* set.



Figure 10. Qualitative segmentation results of MS COCO 2014 *val* set.

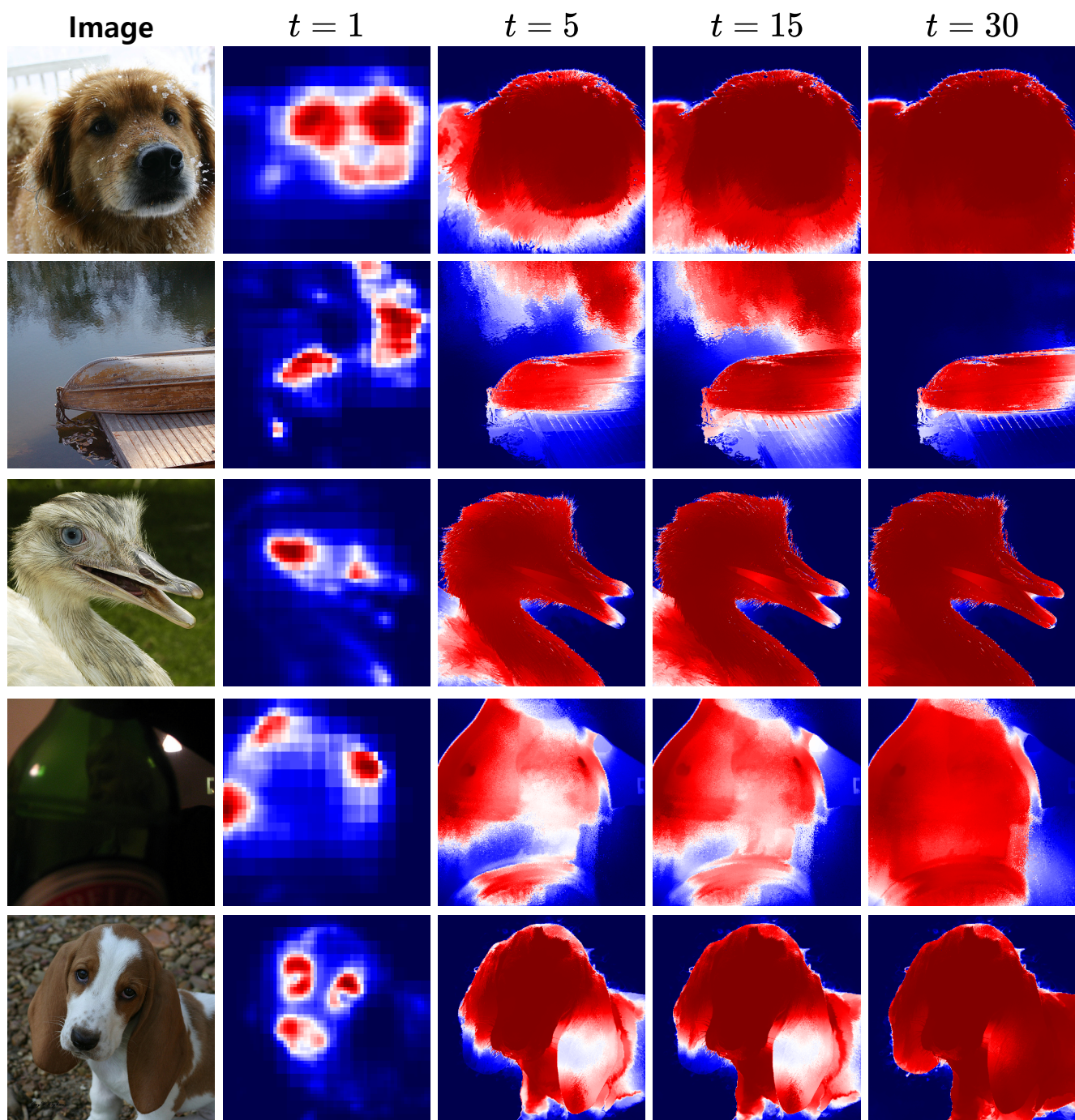


Figure 11. Visualization of attention maps with recursive improvements on the PASCAL VOC 2012 *train* set.

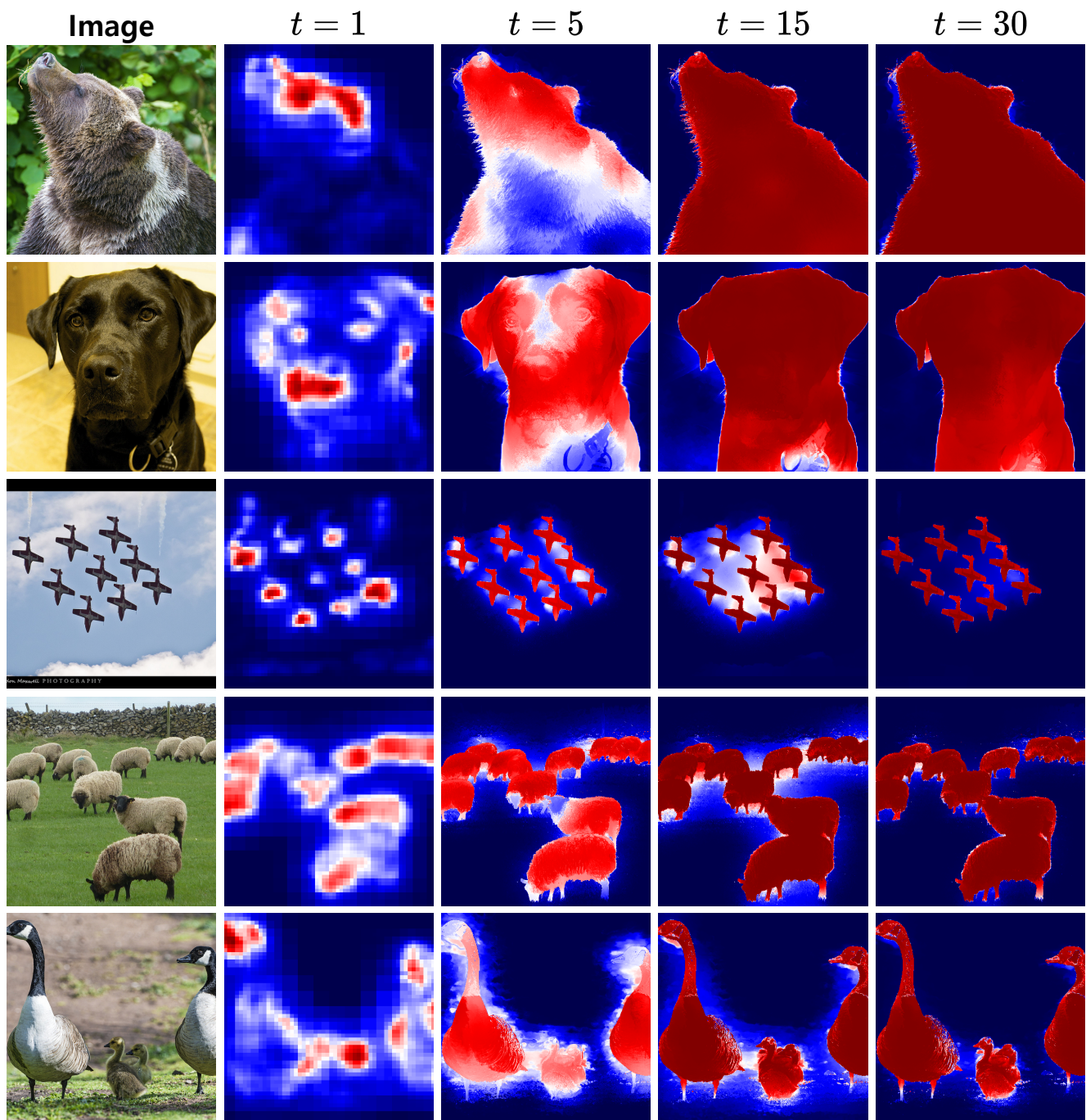


Figure 12. Visualization of attention maps with recursive improvements on the MS COCO 2014 *train* set.

References

- [1] Jiwoon Ahn and Suha Kwak. Learning pixel-level semantic affinity with image-level supervision for weakly supervised semantic segmentation. In *IEEE CVPR*, pages 4981–4990, 2018. [1](#), [2](#), [5](#), [6](#), [11](#)
- [2] Jiwoon Ahn, Sunghyun Cho, and Suha Kwak. Weakly supervised learning of instance segmentation with inter-pixel relations. In *IEEE CVPR*, pages 2209–2218, 2019. [5](#), [6](#), [7](#)
- [3] Nikita Araslanov and Stefan Roth. Single-stage semantic segmentation from image labels. In *IEEE CVPR*, pages 4253–4262, 2020. [1](#), [2](#), [5](#), [6](#), [7](#), [8](#), [9](#), [11](#)
- [4] Amy Bearman, Olga Russakovsky, Vittorio Ferrari, and Li Fei-Fei. What’s the point: Semantic segmentation with point supervision. In *ECCV*, pages 549–565. Springer, 2016. [1](#)
- [5] John Canny. A computational approach to edge detection. *IEEE TPAMI*, pages 679–698, 1986. [4](#), [7](#)
- [6] Liang-Chieh Chen, Yukun Zhu, George Papandreou, Florian Schroff, and Hartwig Adam. Encoder-decoder with atrous separable convolution for semantic image segmentation. In *ECCV*, pages 801–818, 2018. [3](#), [5](#)
- [7] Qi Chen, Lingxiao Yang, Jian-Huang Lai, and Xiaohua Xie. Self-supervised image-specific prototype exploration for weakly supervised semantic segmentation. In *IEEE CVPR*, pages 4288–4298, 2022. [1](#), [2](#), [6](#)
- [8] Zhaozheng Chen, Tan Wang, Xiongwei Wu, Xian-Sheng Hua, Hanwang Zhang, and Qianru Sun. Class re-activation maps for weakly-supervised semantic segmentation. In *IEEE CVPR*, pages 969–978, 2022. [6](#)
- [9] Zesen Cheng, Pengchong Qiao, Kehan Li, Siheng Li, Pengxu Wei, Xiangyang Ji, Li Yuan, Chang Liu, and Jie Chen. Out-of-candidate rectification for weakly supervised semantic segmentation. In *IEEE CVPR*, pages 23673–23684, 2023. [1](#), [2](#), [6](#)
- [10] Ye Du, Zehua Fu, Qingjie Liu, and Yunhong Wang. Weakly supervised semantic segmentation by pixel-to-prototype contrast. In *IEEE CVPR*, pages 4320–4329, 2022. [2](#), [6](#), [7](#)
- [11] Mark Everingham, Luc Van Gool, Christopher KI Williams, John Winn, and Andrew Zisserman. The pascal visual object classes (VOC) challenge. *IJCV*, 88(2):303–338, 2010. [5](#)
- [12] Junsong Fan, Zhaoxiang Zhang, Tieniu Tan, Chunfeng Song, and Jun Xiao. Cian: Cross-image affinity net for weakly supervised semantic segmentation. In *AAAI*, pages 10762–10769, 2020. [11](#)
- [13] Kaiming He, Xiangyu Zhang, Shaoqing Ren, and Jian Sun. Deep residual learning for image recognition. In *IEEE CVPR*, pages 770–778, 2016. [3](#)
- [14] Seunghoon Hong, Junhyuk Oh, Honglak Lee, and Bohyung Han. Learning transferrable knowledge for semantic segmentation with deep convolutional neural network. In *IEEE CVPR*, pages 3204–3212, 2016. [11](#)
- [15] Seunghoon Hong, Donghun Yeo, Suha Kwak, Honglak Lee, and Bohyung Han. Weakly supervised semantic segmentation using web-crawled videos. In *IEEE CVPR*, pages 7322–7330, 2017. [11](#)
- [16] Zilong Huang, Xinggang Wang, Jiasi Wang, Wenyu Liu, and Jingdong Wang. Weakly-supervised semantic segmentation network with deep seeded region growing. In *IEEE CVPR*, pages 7014–7023, 2018. [6](#), [11](#)
- [17] Peng-Tao Jiang, Yuqi Yang, Qibin Hou, and Yunchao Wei. L2G: A simple local-to-global knowledge transfer framework for weakly supervised semantic segmentation. In *IEEE CVPR*, pages 16886–16896, 2022. [2](#), [6](#)
- [18] Sanghyun Jo and In-Jae Yu. Puzzle-CAM: Improved localization via matching partial and full features. In *IEEE ICIP*, pages 639–643. IEEE, 2021. [2](#)
- [19] Beomyoung Kim, Sangeun Han, and Junmo Kim. Discriminative region suppression for weakly-supervised semantic segmentation. In *AAAI*, pages 1754–1761, 2021. [11](#)
- [20] Alexander Kolesnikov and Christoph H Lampert. Seed, expand and constrain: Three principles for weakly-supervised image segmentation. In *ECCV*, pages 695–711. Springer, 2016. [2](#), [11](#)
- [21] Philipp Krähenbühl and Vladlen Koltun. Efficient inference in fully connected CRFs with gaussian edge potentials. *NeurIPS*, 24:109–117, 2011. [5](#), [9](#)
- [22] Hyeokjun Kweon, Sung-Hoon Yoon, Hyeonseong Kim, Daehee Park, and Kuk-Jin Yoon. Unlocking the potential of ordinary classifier: Class-specific adversarial erasing framework for weakly supervised semantic segmentation. In *IEEE ICCV*, pages 6994–7003, 2021. [11](#)
- [23] Hyeokjun Kweon, Sung-Hoon Yoon, and Kuk-Jin Yoon. Weakly supervised semantic segmentation via adversarial learning of classifier and reconstructor. In *IEEE CVPR*, pages 11329–11339, 2023. [1](#), [2](#), [6](#)
- [24] Jungbeom Lee, Eunji Kim, Sungmin Lee, Jangho Lee, and Sungroh Yoon. FickleNet: Weakly and semi-supervised semantic image segmentation using stochastic inference. In *IEEE CVPR*, pages 5267–5276, 2019. [6](#), [11](#)
- [25] Jungbeom Lee, Jooyoung Choi, Jisoo Mok, and Sungroh Yoon. Reducing information bottleneck for weakly supervised semantic segmentation. *NeurIPS*, 34, 2021. [6](#), [7](#), [11](#)
- [26] Jungbeom Lee, Eunji Kim, and Sungroh Yoon. Anti-adversarially manipulated attributions for weakly and semi-supervised semantic segmentation. In *IEEE CVPR*, pages 4071–4080, 2021. [2](#), [6](#), [7](#), [11](#)
- [27] Jungbeom Lee, Seong Joon Oh, Sangdoo Yun, Junsuk Choe, Eunji Kim, and Sungroh Yoon. Weakly supervised semantic segmentation using out-of-distribution data. In *IEEE CVPR*, pages 16897–16906, 2022. [2](#), [6](#)
- [28] Minhyun Lee, Dongseob Kim, and Hyunjung Shim. Threshold Matters in WSSS: Manipulating the activation for the robust and accurate segmentation model against thresholds. In *IEEE CVPR*, pages 4330–4339, 2022. [2](#), [6](#)
- [29] Jing Li, Junsong Fan, and Zhaoxiang Zhang. Towards noiseless object contours for weakly supervised semantic segmentation. In *IEEE CVPR*, pages 16856–16865, 2022. [2](#), [6](#)
- [30] Zhiyuan Liang, Tiancai Wang, Xiangyu Zhang, Jian Sun, and Jianbing Shen. Tree Energy Loss: Towards sparsely annotated semantic segmentation. In *IEEE CVPR*, pages 16907–16916, 2022. [6](#)
- [31] Tsung-Yi Lin, Michael Maire, Serge Belongie, James Hays, Pietro Perona, Deva Ramanan, Piotr Dollár, and C Lawrence Zitnick. Microsoft COCO: Common objects in context. In *ECCV*, pages 740–755. Springer, 2014. [5](#)

- [32] Sheng Liu, Kangning Liu, Weicheng Zhu, Yiqiu Shen, and Carlos Fernandez-Granda. Adaptive early-learning correction for segmentation from noisy annotations. In *IEEE CVPR*, pages 2606–2616, 2022. 2, 6
- [33] Youngmin Oh, Beomjun Kim, and Bumsu Ham. Background-aware pooling and noise-aware loss for weakly-supervised semantic segmentation. In *IEEE CVPR*, pages 6913–6922, 2021. 6
- [34] Viktor Olsson, Wilhelm Trane, Juliano Pinto, and Lennart Svensson. ClassMix: Segmentation-based data augmentation for semi-supervised learning. In *IEEE WACV*, pages 1369–1378, 2021. 1, 2, 7
- [35] Xingjia Pan, Yingguo Gao, Zhiwen Lin, Fan Tang, Weiming Dong, Haolei Yuan, Feiyue Huang, and Changsheng Xu. Unveiling the potential of structure preserving for weakly supervised object localization. In *IEEE CVPR*, pages 11642–11651, 2021. 1, 9
- [36] George Papandreou, Liang-Chieh Chen, Kevin P Murphy, and Alan L Yuille. Weakly-and semi-supervised learning of a deep convolutional network for semantic image segmentation. In *IEEE ICCV*, pages 1742–1750, 2015. 11
- [37] Joonhyung Park, June Yong Yang, Jinwoo Shin, Sung Ju Hwang, and Eunho Yang. Saliency Grafting: Innocuous attribution-guided mixup with calibrated label mixing. In *AAAI*, pages 7957–7965, 2022. 2, 7
- [38] Pedro O Pinheiro and Ronan Collobert. From image-level to pixel-level labeling with convolutional networks. In *IEEE CVPR*, pages 1713–1721, 2015. 11
- [39] Jie Qin, Jie Wu, Xuefeng Xiao, Lujun Li, and Xingang Wang. Activation modulation and recalibration scheme for weakly supervised semantic segmentation. In *AAAI*, pages 2117–2125, 2022. 6
- [40] Shenghai Rong, Bohai Tu, Zilei Wang, and Junjie Li. Boundary-enhanced co-training for weakly supervised semantic segmentation. In *IEEE CVPR*, pages 19574–19584, 2023. 2, 6
- [41] Azriel Rosenfeld and John L Pfaltz. Sequential operations in digital picture processing. *Journal of the ACM (JACM)*, 13(4):471–494, 1966. 4, 10
- [42] Anirban Roy and Sinisa Todorovic. Combining bottom-up, top-down, and smoothness cues for weakly supervised image segmentation. In *IEEE CVPR*, pages 3529–3538, 2017. 1, 11
- [43] Lixiang Ru, Yibing Zhan, Baosheng Yu, and Bo Du. Learning affinity from attention: end-to-end weakly-supervised semantic segmentation with transformers. In *IEEE CVPR*, pages 16846–16855, 2022. 2, 6, 7, 8
- [44] Lixiang Ru, Heliang Zheng, Yibing Zhan, and Bo Du. Token contrast for weakly-supervised semantic segmentation. In *Proceedings of the IEEE/CVF Conference on Computer Vision and Pattern Recognition*, pages 3093–3102, 2023. 1, 2, 6, 8
- [45] Wataru Shimoda and Keiji Yanai. Self-supervised difference detection for weakly-supervised semantic segmentation. In *IEEE ICCV*, pages 5208–5217, 2019. 11
- [46] Yukun Su, Ruizhou Sun, Guosheng Lin, and Qingyao Wu. Context decoupling augmentation for weakly supervised semantic segmentation. In *IEEE ICCV*, pages 7004–7014, 2021. 2, 6, 7
- [47] Guolei Sun, Wenguan Wang, Jifeng Dai, and Luc Van Gool. Mining cross-image semantics for weakly supervised semantic segmentation. In *ECCV*, pages 347–365. Springer, 2020. 2, 11
- [48] Yude Wang, Jie Zhang, Meina Kan, Shiguang Shan, and Xilin Chen. Self-supervised equivariant attention mechanism for weakly supervised semantic segmentation. In *IEEE CVPR*, pages 12275–12284, 2020. 2, 5, 6, 7, 11
- [49] Tong Wu, Junshi Huang, Guangyu Gao, Xiaoming Wei, Xiaolin Wei, Xuan Luo, and Chi Harold Liu. Embedded discriminative attention mechanism for weakly supervised semantic segmentation. In *IEEE CVPR*, pages 16765–16774, 2021. 2, 6, 11
- [50] Jinheng Xie, Xianxu Hou, Kai Ye, and Linlin Shen. CLIMS: Cross language image matching for weakly supervised semantic segmentation. In *IEEE CVPR*, pages 4483–4492, 2022. 2, 6
- [51] Jinheng Xie, Jianfeng Xiang, Junliang Chen, Xianxu Hou, Xiaodong Zhao, and Linlin Shen. C2AM: Contrastive learning of class-agnostic activation map for weakly supervised object localization and semantic segmentation. In *IEEE CVPR*, pages 989–998, 2022. 2
- [52] Saining Xie and Zhuowen Tu. Holistically-nested edge detection. In *IEEE ICCV*, pages 1395–1403, 2015. 7
- [53] Lian Xu, Wanli Ouyang, Mohammed Bennamoun, Farid Boussaid, and Dan Xu. Multi-class token transformer for weakly supervised semantic segmentation. In *IEEE CVPR*, pages 4310–4319, 2022. 2, 6
- [54] Yazhou Yao, Tao Chen, Guo-Sen Xie, Chuanyi Zhang, Fumin Shen, Qi Wu, Zhenmin Tang, and Jian Zhang. Non-salient region object mining for weakly supervised semantic segmentation. In *IEEE CVPR*, pages 2623–2632, 2021. 11
- [55] Sangdoo Yun, Dongyoon Han, Seong Joon Oh, Sanghyuk Chun, Junsuk Choe, and Youngjoon Yoo. CutMix: Regularization strategy to train strong classifiers with localizable features. In *IEEE ICCV*, pages 6023–6032, 2019. 2, 7
- [56] Bingfeng Zhang, Jimin Xiao, Yunchao Wei, Mingjie Sun, and Kaizhu Huang. Reliability Does Matter: An end-to-end weakly supervised semantic segmentation approach. In *AAAI*, pages 12765–12772, 2020. 1, 2, 6, 7, 8, 11
- [57] Dong Zhang, Hanwang Zhang, Jinhui Tang, Xian-Sheng Hua, and Qianru Sun. Causal intervention for weakly-supervised semantic segmentation. *NeurIPS*, 33:655–666, 2020. 6, 7, 11
- [58] Fei Zhang, Chaochen Gu, Chenyue Zhang, and Yuchao Dai. Complementary patch for weakly supervised semantic segmentation. In *IEEE ICCV*, pages 7242–7251, 2021. 2, 7, 11
- [59] Bolei Zhou, Aditya Khosla, Agata Lapedriza, Aude Oliva, and Antonio Torralba. Learning deep features for discriminative localization. In *IEEE CVPR*, pages 2921–2929, 2016. 1
- [60] Tianfei Zhou, Meijie Zhang, Fang Zhao, and Jianwu Li. Regional semantic contrast and aggregation for weakly supervised semantic segmentation. In *IEEE CVPR*, pages 4299–4309, 2022. 1, 2, 6